Self-consistent removal of sawtooth oscillations from transient plasma data by Generalized Singular Value Decomposition

T. Dudok de Wit[1], M. Erba[2], M. Mattioli[2] and J.-L. Ségui[2]

[1] Centre de Physique Théorique, Luminy, case 907, 13288 Marseille cedex 9, France

[2] Association Euratom-CEA sur la Fusion, CEN Cadarache, 13108 St.Paul-lez-Durance cedex, France

Abstract

This paper addresses the problem of removing sawtooth oscillations from multichannel plasma data in a self-consistent way, thereby preserving transients that have a different physical origin. The technique which does this is called the Generalized Singular Value Decomposition (GSVD), and its properties are discussed. Using the GSVD, spatially resolved electron temperature measurements are analyzed. Special attention is paid to transient regimes in which the temperature is perturbed either by the laser blow-off injection of impurities or by pellet injection. Non-local transport issues are briefly discussed.

1 Introduction

A basic problem in experimental physics is the extraction of the dynamics of a system which is polluted by some uncontrollable but known perturbation (hereafter called *noise*). A generic example in fusion plasmas is given by sawtooth oscillations, whose continuous modulation considerably hinders the analysis of transient events such as propagating heat fronts. There are different ways such perturbations can be removed from the observations. The usual approach is based on linear filtering, but this works only if the noise and the dynamics of interest have sufficiently different power spectral densities. A recent and powerful alternative involves filtering in phase or state space; this approach is particularly effective when assumptions can be made on the system or noise dynamics. Low dimensional chaotic systems, for example, can be efficiently processed that way [1].

Here, we use such a phase space approach to address the longstanding problem of removing sawtooth-induced perturbations from transient plasma data. The approach is based on a linear technique, called Generalized Singular Value Decomposition (GSVD). It is applied to spatially resolved electron temperature measurements made on the Tore Supra [2] tokamak; we focus on stationary discharges in which Ni impurities or H pellets were injected. The transient response of the electron temperature to these stimuli is of great interest since it reveals properties of the underlying transport processes. Their analysis, however, is often compromised by the omnipresence of sawtooth oscillations, which generally mask it and cannot be eliminated without smearing out the dynamical response of the plasma. This problem is particularly acute in perturbative transport experiments, in which the plasma response immediately following the perturbation is of key importance for a proper assessment of the underlying transport processes.

In this paper, we show how this problem can be overcome by applying the GSVD technique, which removes the sawtooth contribution self-consistently and thereby preserves fast transients for further analysis. Non-local transport aspects can then be investigated in more detail.

Table 1: The main parameters of the four discharges analyzed in this paper: type of perturbation applied to the plasma, plasma current, central electron density, safety factor at the plasma edge, relative central electron temperature change induced by the perturbation, and activation of the ergodic divertor

shot number	20601	20792	21425	21429
perturbation	Ni impurity	Ni impurity	Ni impurity	H pellet
I_p [MA]	1.4	1.15	1	1
$n_{eo}[10^{19}\mathrm{m}^{-3}]$	4.9	3.3	1.6	1.6
q_a	3.2	3.0	5.6	5.6
$\Delta T_{eo}/T_{eo}$	-6 %	-16 %	$< +5$ %	-30 %
ergodic divertor	on	off	off	off

2 Description of the experiments

The injection of a small amount of matter has for more than a decade been a standard method for studying transient transport in plasmas. The recent debate on non-local transport has revived the interest in such perturbative experiments after it was shown on different tokamaks [3, 4, 5, 6, 7, 8] that the core electron temperature reacts almost instantaneously to the ablation at the edge, an effect that cannot not be satisfactorily explained in terms of a local action of the inward propagating impurities. In some cases, and most surprisingly, the edge cooling even leads to a central electron temperature rise [3, 4, 6, 7].

These scenarii have been reproduced on the Tore Supra tokamak, in which metal impurities were injected by laser blow-off in stationary discharges [9, 10]. The electron temperature T_e is measured by a 16-channel electron cyclotron heterodyne radiometer[11]; its temporal resolution is 1 ms and 12 or 13 innermost channels out of 16 are used. Tore Supra is a supraconducting tokamak with a circular cross-section, major radius $R = 2.25 - 2.4$ m and a limiter radius $a = 0.70 - 0.78$ m. Table 1 lists the main plasma parameters of the four discharges we'll be studying in this paper.

In shots #20601, #20792, and #21425, the plasma is weakly perturbed by the injection of a small amount of Ni whose cooling effect results in a small but measurable temperature modification throughout the plasma column [10]. The activation of the ergodic divertor in shot #20601 modifies the electron density at the plasma edge, thereby screening off the intrinsic impurities, reducing the turbulence level and enhancing the radiative power fraction in that region [12].

Two examples of the time evolution of the electron temperature are given in Figs. 1 and 2. The global behavior is identical to that reported on other tokamaks, namely with an inward propagating cold front. Simultaneous measurements of the soft X-ray emission indicate that the impurities and the cold front initially propagate together, as would be expected from a radiation enhanced cooling. Inside the inversion radius, however, the temperature starts to change well before the influx of the impurities, whose penetration is mediated by the sawtooth activity [10]. This inconsistency with the usual picture of a local action of the impurity flux has been attributed to non-local transport mechanisms.

Clearly, a reliable assessment of the differential propagation velocity in the plasma core heavily relies on our ability to resolve the initial transient following the laser blow-off pulse. This provides a strong motivation for filtering out the sawtooth modulation in such a way that the impurity-induced perturbation is preserved. Filtered data are also needed for a more reliable quantification of the plasma relaxation times.

The processes we deal with are intrinsically nonlinear, but since we consider small deviations from an equilibrium state, there is a good chance that a simple linear analysis may do well in separating them. Indeed, neither the sawtooth period nor its propagation through the plasma are strongly affected by the impurity injection. This is not the case anymore with shot #21429, in which a H pellet

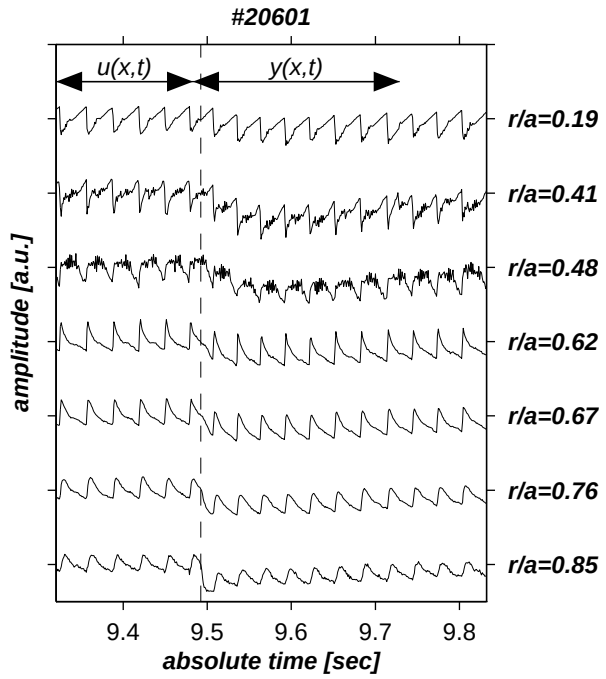

Figure 1: Time evolution of the electron temperature for shot #20601 with impurity injection. The dashed line indicates the injection time and 7 channels only out of 12 are shown; amplitudes are in arbitrary units.

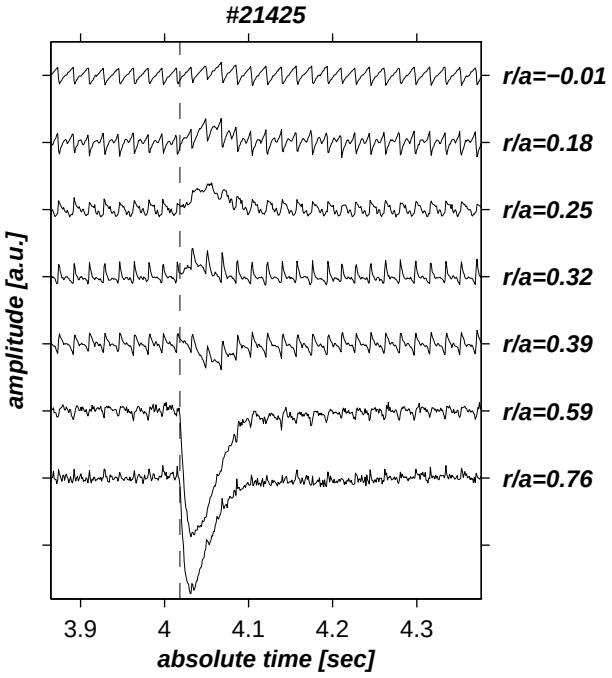

Figure 2: Time evolution of the electron temperature for shot #21425 with impurity injection. Note the central electron temperature rise; amplitudes are in arbitrary units.

perturbs the plasma more significantly and affects the sawtooth oscillations, see Fig. 3. In this example, the plasma response and the sawtooth dynamics are deeply intertwined, making a complete separation more difficult. This will be confirmed below by the (partial) failure of a GSVD analysis.

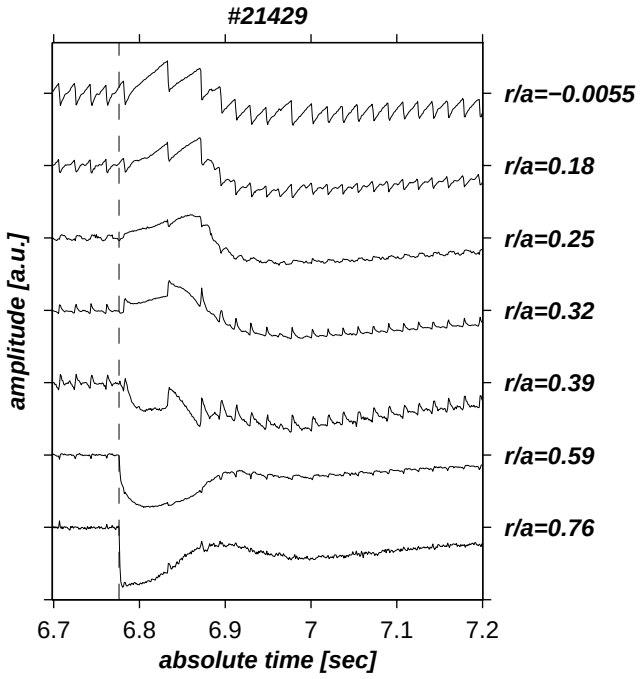

Figure 3: Time evolution of the raw electron temperature for shot #21429, in which a pellet is injected; amplitudes are in arbitrary units.

3 A phase space representation of the data

The main requirement for a GSVD analysis is the possibility to make two different observations of the same system: one with the noisy dynamics of interest and one with merely noise. Remember that *noise* here has a broad meaning since it designates any known perturbation we want to disregard from our observations. This definition encompasses coherent oscillations such as magnetohydrodynamic (MHD) modes and incoherent instrumental noise.

The GSVD is best understood in terms of a phase space representation, which we now briefly present. Consider an experiment whose time-evolution is recorded by means of different diagnostics or a multichannel diagnostic, giving an ensemble of measurements $\{y_1(t), y_2(t), \cdots, y_d(t)\}$. The collection of points whose coordinates are $(y_1(t), y_2(t), \cdots, y_d(t))$ defines a trajectory in d-dimensional phase space. Each state of the system corresponds to a point on that trajectory while the time evolution is depicted qualitatively by the way the trajectories move away these points. This representation provides a starting point for various powerful concepts that were initially developed in the framework of dynamical systems [13, 14] and later applied to nonlinear time series analysis [15, 16].

The main point here is that processes with different dynamics evolve along different trajectories. States that are associated with deterministic processes tend to cluster in reproducible trajectories [17] whereas stochastic processes (e.g. incoherent noise) merely yield clouds of scattered points [14]. The idea then consists in finding a basis that enhances the representation of those trajectories we are interested in while capturing the least possible of the unwanted ones. Such a basis is not necessarily related to the system eigenmodes (if there are any) since it depends on the system and on what

we define as noise. Clearly, the degree of separation that can be achieved depends on our ability to distinguish different dynamics.

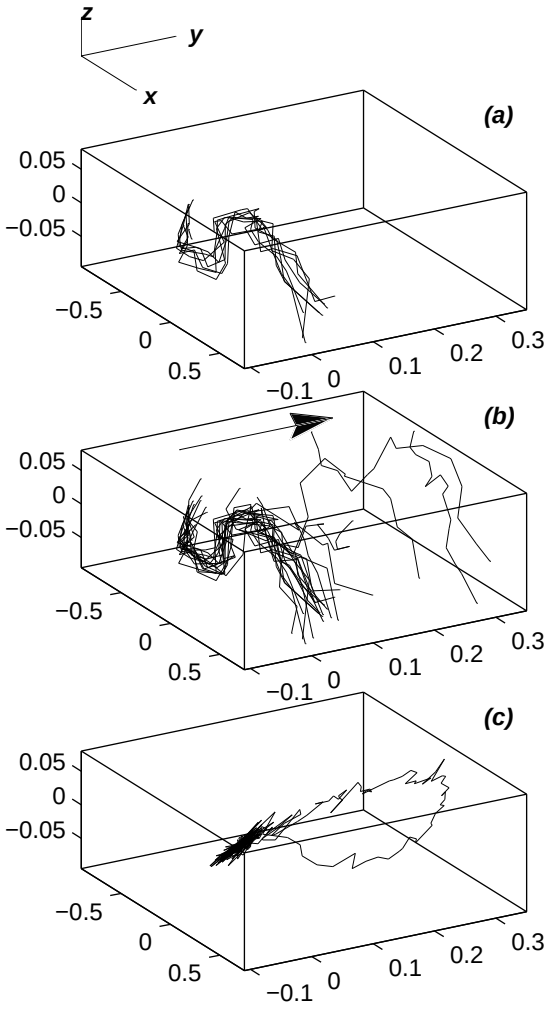

Figure 4: Representation of the trajectories in a 3-D phase space for shot #20792. The coordinates of the trajectories are $(x, y, z) = (T_e(t, r/a = 0.05), T_e(t, r/a = 0.25), T_e(t, r/a = 0.18))$. Figure (a) shows the trajectory associated with sawtooth modulations in a stationary regime. In Figure (b), using the same basis, we observe both sawteeth and a perturbation caused by the injection of impurities. The same event is displayed in (c), but the trajectories are now projected along 3 dominant modes of the GSVD. In this new representation, a completely different trajectory (x', y', z') appears, in which the sawtooth modulation is barely perceptible.

The plasma electron temperature is probed at 12 different locations, so the associated phase space is 12-dimensional. This does not necessarily mean, however, that the dimensionality of the trajectories is as high. Indeed, the intrinsic dimension is often lower; in our case a 3-D projection with suitably chosen axes already suffices for capturing most of the pertinent features. Such a 3-D phase space is illustrated in Fig. 4a for a stationary regime with sawtooth modulations only. Each axis corresponds to one particular channel of the diagnostic; we have chosen here a central one, a channel located just outside the inversion radius, and a more peripheral channel. The coordinates of the trajectories thus correspond to $(T_e(t, r_a), T_e(t, r_b), T_e(t, r_c))$. The presence of reproducible trajectories, by analogy with the properties of dynamical systems, clearly attests the deterministic nature

of the sawtoothing process, in the sense that the spatio-temporal dynamics of a stationary regime can reasonably well be cast into an equation of the type

$$\frac{\partial T_e(t, r_i)}{\partial t} = F\left[T_e(t, r_1), T_e(t, r_2), \cdots, T_e(t, r_{12})\right] \tag{1}$$

$\forall t$ and for $i = 1, 2, \ldots, 12$. In Fig. 4b the same representation is extended to a regime in which sawteeth and an impurity-induced perturbation coexist. The latter causes a sudden displacement of the trajectories, which subsequently relax to the original ones. Notice how the trajectories are displaced almost perpendicularly to the plane they normally belong to. This suggests that any projection along a direction perpendicular to that plane (shown in Fig. 4b) should mostly reveal the slow relaxation and conversely capture little of the sawtooth-related oscillation. The GSVD technique chooses such directions in an optimal way, to be defined below. A new basis is obtained, on which the trajectories can be projected. A projection on three such basis vectors is illustrated in Fig. 4c, clearly showing how the sawtooth-related modulation has been almost completely eliminated, leaving the slow impurity-induced relaxation only. In this example a linear separation between the two concurrent processes is achieved simply by choosing a suitable projection.

To remove the sawtooth modulation from the original data, we now proceed backwards by keeping the k projections that interest us and setting the $d - k$ other ones to zero. The trajectories are then transformed back into their original coordinate system, giving the "filtered" time series. We must stress that this operation is not equivalent to a filtering in Fourier space since it preserves fast transients. In particular, any discontinuity whose effect on the plasma differs from that of a sawtooth pulse, will be preserved.

To summarize, there are two basic assumptions we make with the GSVD:

1. The sawtooth oscillations and the transients generated by the injections do not have the same dynamics: they propagate differently and have different source terms. Indeed, a perturbation propagating exactly like a sawtooth pulse would be identified as such even if it had a different physical origin.

2. The sawtooth oscillations are not strongly affected by the perturbation we want to study (the reverse does not have to be true). This means that the sawtooth amplitude and period may vary self-consistently, but not their propagation through the plasma. More exotic phenomena such as compound or double sawteeth are not excluded by this.

4 The GSVD

The first step in a GSVD analysis is the reconstruction of the phase space. As shown before, this is easily done with multichannel data [18]. Sometimes, only a single time series is available or the intrinsic dimension of the trajectories exceeds the number of probes or variables. In those cases, the possibility to unfold the geometrical structure of the phase space is still ensured by Takens' embedding theorem [1, 13]. Let the vector $y(t) = [y(t_0),\ y(t_1),\ y(t_2),\ \cdots]^T$ designate a scalar time series sampled at a constant rate. The trajectory matrix, which contains lagged versions of the same vector

$$Y = [y(t),\ y(t + \tau),\ \cdots,\ y(t + d\,\tau)] \tag{2}$$

then defines a trajectory of the system in a d-dimensional space. The optimal choice of the delay τ and dimension d have been the object of numerous investigations [1, 15, 16] and will not be addressed here. This embedding procedure may be combined with multichannel data if necessary to further unfold the trajectories.

In view of future applications and without loss of generality, we'll assume that our data are of the multichannel type, each channel corresponding to a location in space. The (i, j)'th element of the trajectory matrix then equals $Y_{ij} = y(x_j, t_i)$ and the dimension d is set by the number of channels. Furthermore, since one is generally interested in transients only, all time averages are removed

beforehand $\langle y(x,t)\rangle_t = 0$. Let $y(x,t)$ now denote the noisy observations and $u(x,t)$ the noise dominated ones. The recording conditions (location and number of probes, sampling period, etc.) have to be the same for both experiments, but the number of samples don't.

Our phase space may not yet be optimal for analysis purposes and a different basis can often ease the analysis. The Singular Value Decomposition (SVD), also known as the Karhunen-Loève transform, Principal Component Analysis or Biorthogonal Decomposition, does this by rotating the phase space into a new coordinate system whose orthogonal axes $\{v_k(x)\}$ coincide with the axes of inertia of the data [19, 20, 21]. In this new basis, the spatio-temporal observables are decomposed into a unique set of orthonormal spatial and temporal modes

$$y(x,t) = \sum_{k=1}^{K} \alpha_k \, a_k^*(t) \, v_k(x) \tag{3}$$

with $\langle a_k^* a_l \rangle = \langle v_k^* v_l \rangle = \delta_{kl}$ (* stands for complex conjugation and δ_{kl} is the Kronecker symbol) and by convention the modes are ordered so that $\alpha_1 \geq \alpha_2 \geq \cdots \geq \alpha_K \geq 0$. The dimension K of the phase space is the smallest of the number of samples or probes; since the latter situation is the generic one, we'll take here $K = d$. If the phase space has structured trajectories, that is, if the observations are correlated in time and in space, then a few weights α_k usually dominate the expansion. One can then project most of the pertinent dynamics on a few dominant modes only and thereby truncate the expansion at $L \leq K$. This property of the SVD has been successfully used to build Galerkin bases for large-dimensional systems [22, 23] and to characterize spatio-temporal patterns in laboratory plasmas [24, 25, 26, 27].

The GSVD [19, 28, 29] exploits the same idea as the SVD, but with a basic difference: it gives a common basis for $y(x,t)$ and $u(x,t)$ that optimizes the representation of the former while capturing the least possible of the latter. This basis is again complete and unique

$$\begin{aligned} y(x,t) &= \sum_{k=1}^{K} \alpha_k \, a_k^*(t) \, v_k(x) \\ u(x,t) &= \sum_{k=1}^{K} \beta_k \, b_k^*(t) \, v_k(x) \end{aligned} \tag{4}$$

but not necessarily orthogonal : in general $\langle v_k^* v_l \rangle \neq 0$ for $k \neq l$. The temporal modes, however, are orthonormal. By convention, the weights are normalized by $\alpha_k^2 + \beta_k^2 = 1$. Because of this they are sometimes interpreted as cosines and sines of the angles between the two subspaces. The elements $\{\sigma_k\} = \{\alpha_k/\beta_k\}$, which are again all positive and sorted in decreasing order, are referred to as the generalized singular values of $y(x,t)$ and $u(x,t)$. In a signal processing framework they are called oriented signal-to-signal ratios because each generalized singular value squared σ_k^2 is equal to the ratio of the variances of $y(x,t)$ and $u(x,t)$ along the direction given by the spatial basis vector v_k. These basis vectors are chosen in such a way that the largest generalized singular value σ_1 is maximized and the smallest one σ_K minimized. The GSVD thus projects the trajectories on a new basis whose first axes preferentially capture $y(x,t)$ and conversely the last axes reveal $u(x,t)$. The technique is used in numerical analysis for total least squares problems [30] but the phase space separation property has to the best of our knowledge only been exploited in medical engineering applications [31].

A clear ordering of the generalized singular eigenvalues attests the presence of different types of trajectories and thus suggests the possibility to separate them into a "noise" and a "signal" subspace. Indeed, the truncated expansion

$$\hat{y}(x,t) = \sum_{k=1}^{L \leq K} \alpha_k \, a_k^*(t) \, v_k(x) \tag{5}$$

retains most of the desired dynamics while rejecting a sizeable fraction of the noise. Conversely, by symmetry we can isolate the noise by discarding some of the leading modes.

It can be shown [19] that the generalized eigenvalues and the basis functions are solutions of the symmetric eigenvalue problem, which reads in matrix notation

$$\langle Y^*Y\rangle v_k = \sigma_k^2 \langle U^*U\rangle v_k \tag{6}$$

Although the basis functions can be easily calculated that way, it is numerically safer to avoid computing the grammians $\langle Y^*Y\rangle$ and $\langle U^*U\rangle$ and use instead the robust GSVD algorithm [32, 33]. Notice that the structure of Eq. (6) is reminiscent of prewhitening operations used in statistics, such as the Mahalanobis transform. This equation also tells us that the ordinary SVD can be recovered when $u(x,t)$ consists of white noise (i.e. it is neither correlated in time nor in space) since we then have $\langle U^*U\rangle = 1$.

We must stress here that the SVD and the GSVD provide a *linear* transformation and hence are formally not appropriate for nonlinear analysis purposes. They cannot disentangle structures that are nonlinearly correlated and whose trajectories in phase space are not confined to a hyperplane [34]. However, it is also known that a manifold with nonzero curvature can locally be approximated by its tangent plane, on which the GSVD is applicable. Such a linearization will be justified in the examples that follow.

5 Removing sawtooth oscillations with weak perturbations

There are a priori good reasons to believe that impurity injection experiments lend themselves to a GSVD analysis since the induced perturbations are relatively weak. The noise and signal subsets are chosen in the following way. The 200 samples immediately preceding the injection (representing approximately 6 to 8 sawtooth periods) define the noise subset $u(x,t)$ and the 240 subsequent ones define $y(x,t)$, see Fig. 1. These subsets are large enough to give detailed trajectories, but more samples would be needed if the signal-to-noise ratio were lower.

Since we deal here with small deviations from an equilibrium value, it is natural to preprocess the data by subtracting from each channel the average temperature prior to the injection. Unfortunately, neither the GSVD nor the SVD are scale-invariant, and so the outcome depends on the normalization. There is no general recipe for normalizing the data but it is advisable to remove time-averages and have approximately equal noise variances in all channels. In addition, if the two subsets have different numbers of samples N then it is safer to give them equal weights by dividing each set by $\sqrt{N}$.

The result of the GSVD for shot #20792 is partly expressed by the distribution of the generalized singular eigenvalues σ_k, see Fig. 5. From the eigenvalues, we can define a signal-to-signal ratio

$$\mathrm{S}SR_k = 20\log_{10}\frac{\alpha_k}{\beta_k} = 20\log_{10}\sigma_k \tag{7}$$

whose units are decibels. A more geometric interpretation stems from the angular separation between the two subspaces

$$\theta_k = \arctan\frac{\alpha_k}{\beta_k} = \arctan\sigma_k \tag{8}$$

with $0 \le \theta_k \le \pi/2$ since $0 \le \alpha_k \le 1$ and $0 \le \beta_k \le 1$. There is no universal rule for separating the signal and noise subspaces on the basis of these global quantities only. We nevertheless can give some general prescriptions:

1. A good separation can only be achieved with basis vectors whose angular separation θ_k is either close to $\pi/2$ (signal with little noise) or close to 0 (noise with little signal).

2. Angles around $\pi/4$ and signal-to-signal ratios in the vicinity of 0 dB correspond to directions along which the noise and signal subspaces are hard to separate. These directions are usually difficult to handle.

3. The faster the angular distribution drops from $\pi/2$ to 0, the better the separability.

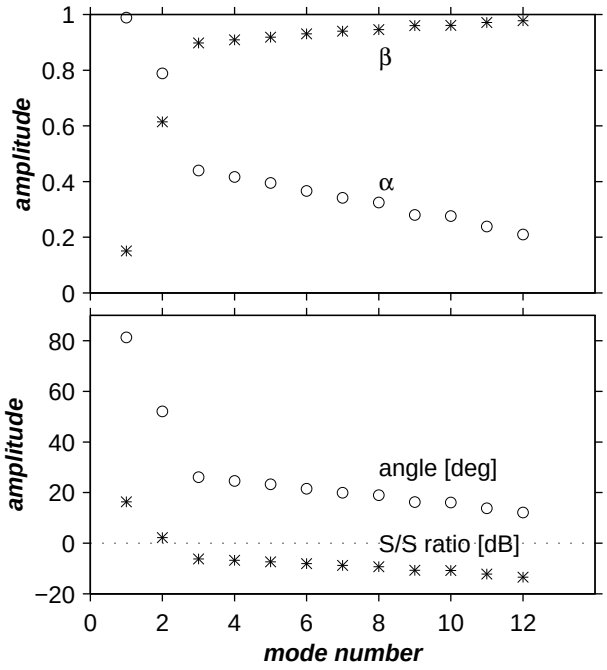

Figure 5: The generalized singular eigenvalues and related quantities for shot #20792. The upper figure shows the weights α_k and β_k. The lower figure displays the corresponding oriented signal-to-signal ratios and separation angles.

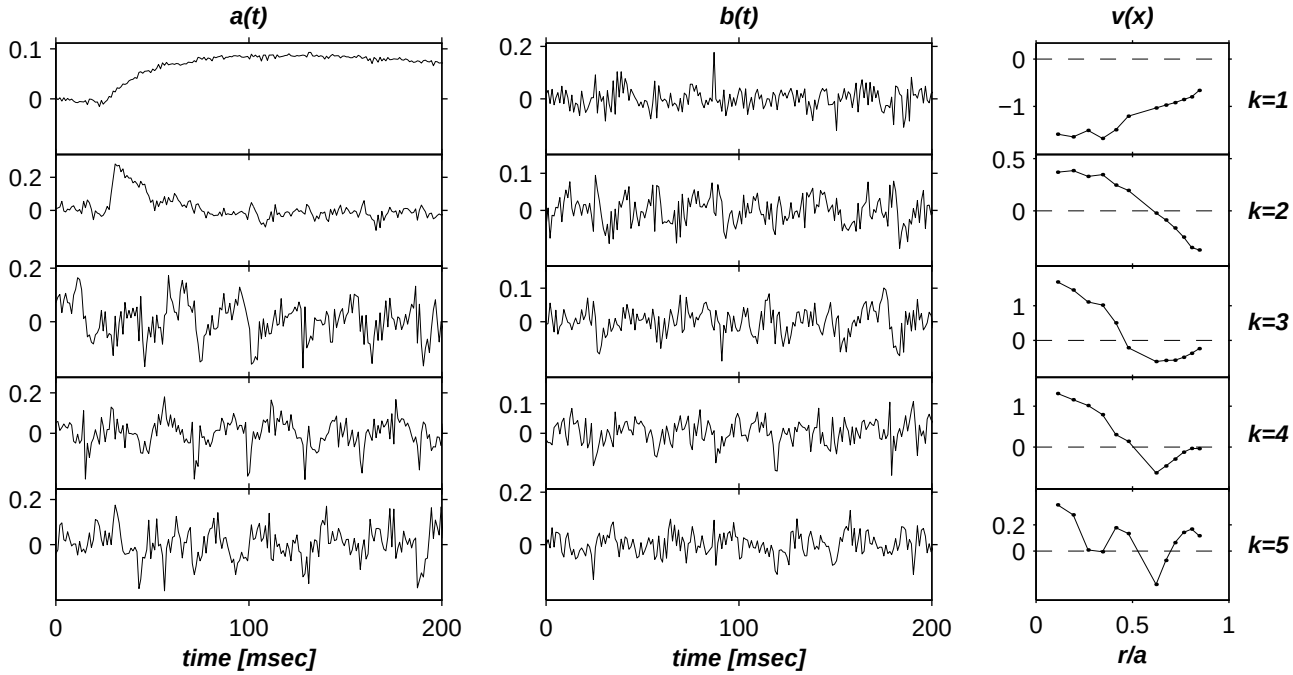

Figure 6: The 5 dominant modes associated with the GSVD for shot #20792. From left to right: the temporal modes $a_k(t)$ of the signal subset, the temporal modes $b_k(t)$ of the noise subset, and the basis vectors $v_k(x)$.

An analysis of the separation angle or of the SSR suffices when the two processes separate easily. If this is not the case a visual inspection of the temporal and spatial modes is recommended.

According to these prescriptions, most of the noiseless dynamics in shot #20792 should be captured by the two dominant directions only. This is indeed confirmed by an inspection of the temporal modes $a_k(t)$ and $b_k(t)$, see Fig. 6. The first two modes reveal the impurity-induced temperature drop without any contribution from the sawtooth modulation. The subsequent modes in contrast reveal sawtooth oscillations but no signature of the injection. The same holds for shots #20601 and #21425.

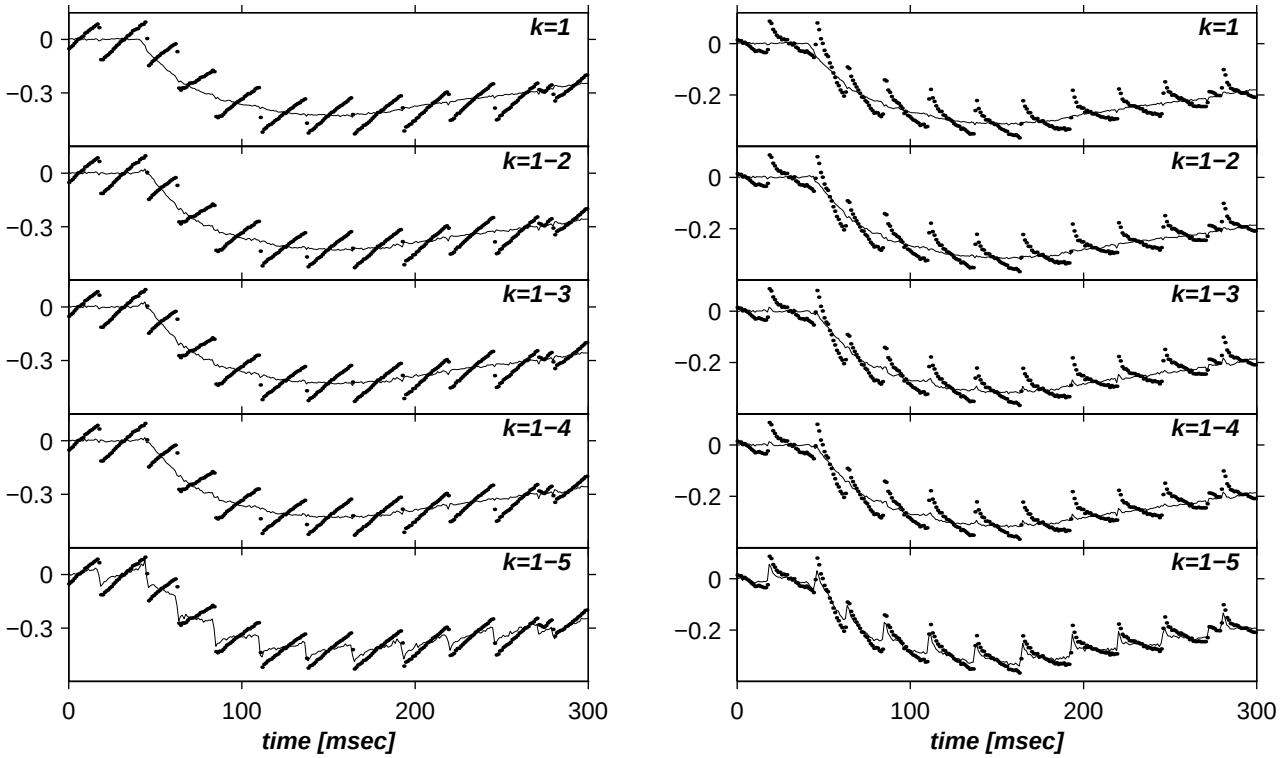

Figure 7: Time evolution of the central (left) and the peripheral (right) electron temperature for shot #20792. Dots correspond to raw data and the thin lines to the temperature as reconstructed using respectively 1 up to 5 of the dominant GSVD modes. Modes 1 and 2 essentially contribute to the temperature relaxation while the subsequent ones do nothing but add sawtooth modulations.

Now that the separability between the noise and signal subspaces has been demonstrated we can attempt a reconstruction of the sawtoothless dynamics by taking a selection of the dominant modes. Fig. 7 shows how satisfactory reconstructions can be already achieved with one mode only. Two modes improve the initial temperature transient a little. With more than two modes the improvement stops and sawtooth-related noise becomes significant. One may thus safely conclude that the GSVD succeeds in eliminating the contribution of the sawteeth, using a projection on two modes only out of twelve. Analyses carried out on numerically simulated data fully support this conclusion.

6 Fast penetration of the cold front

After this brief validation of the GSVD, an investigation of non-local transport aspects in sawtoothing discharges is in order. The main results are summarized in Fig. 8, which displays the filtered time evolution of the electron temperature immediately following the impurity injection for shots #20601, #20792 and #21425. In all of them the cold front propagation can now be observed with unprecedented clarity.

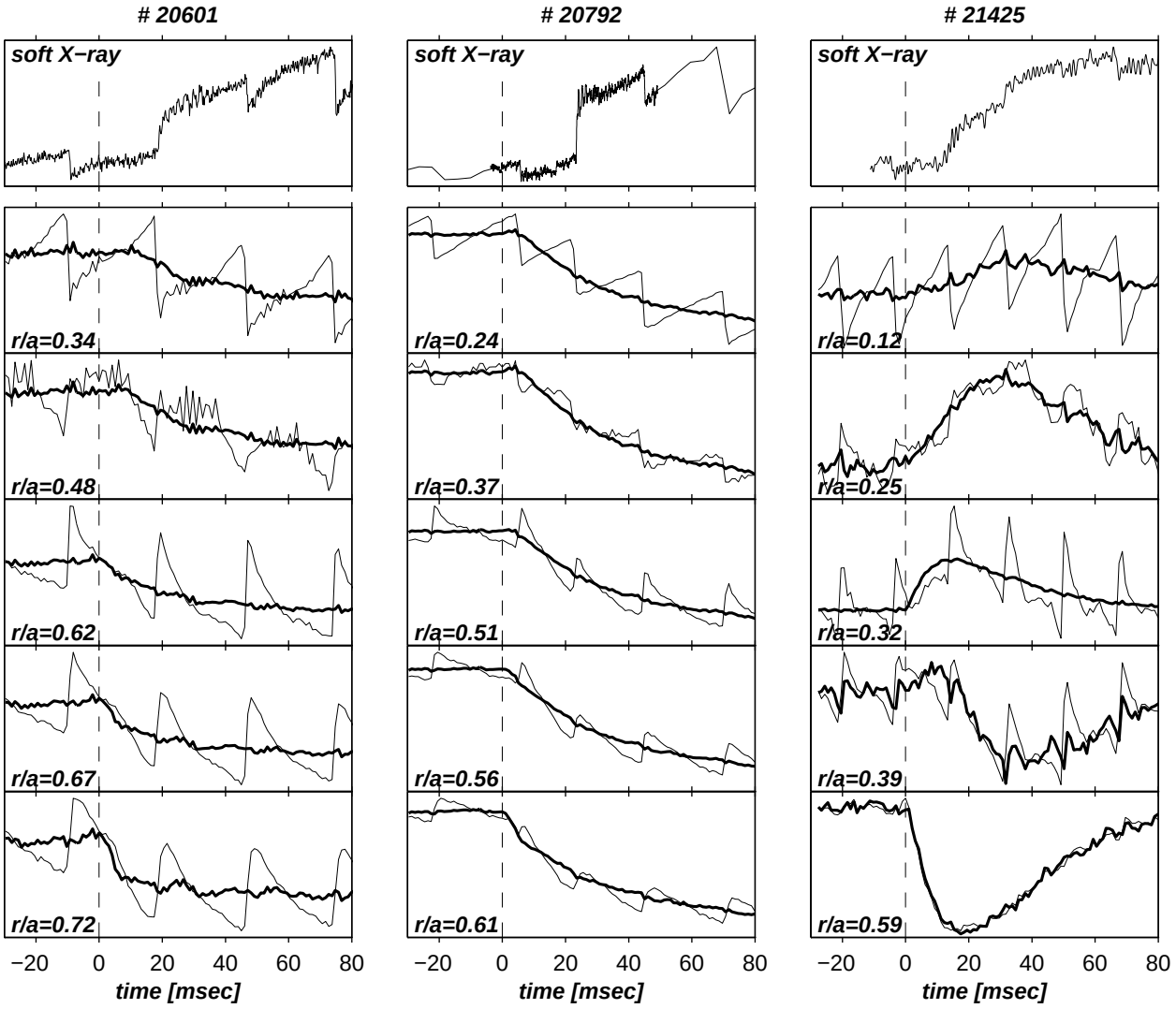

Figure 8: Excerpt of the time evolution of the electron temperature, showing the data before (thick lines) and after GSVD filtering (thin lines). The top row in addition shows the simultaneous evolution of the Abel-inverted central soft X-ray emission. The dashed line marks the impurity injection pulse. Notice the fast reaction of the electron temperature and the delayed inverted sawtooth crash which is the signature of the penetration of the impurities inside the inversion radius. The filtered temperature has been reconstructed using two dominant GSVD modes (three for shot #21425). The amplitudes are in arbitrary units.

Several results are noteworthy. The initial inward propagation of the cold front is fast as it reaches the inversion radius 2 to 5 ms only after the ablation. It takes about the same amount of time for the central electron temperature to react, which is extremely short as compared to the time needed for the impurities the reach the core. Indeed, the penetration of the impurities inside the inversion radius is mediated by the sawtoothing process; its distinctive signature is an inverted sawtooth crash appearing in the soft X-ray emission [10]. The first inverted crash following the ablation occurs at least 10 ms after the temperature has started to change, indicating that the central temperature modification is not due to a radiation increase caused by the influx of impurities.

Another illustration of the differing behavior of the central heat and particle transport processes

is given by shot #20601, in which the central temperature starts to change *during* a sawtooth ramp and is not affected by the subsequent crashes. We checked that this could not be an artifact of the GSVD analysis, since it persists when more modes are used to reconstruct the dynamics. It cannot be attributed to a partial sawtooth either, since none are observed in the central soft X-ray emission.

At lower densities, the dynamical response completely changes as the peripheral cooling causes the core to warm up (shot #21425). This effect is best observed in the contour plot of Fig. 9, in which the fast temperature rise just outside the inversion radius and its subsequent penetration inside the core are readily apparent once the sawteeth have been filtered out. Here again, the impurities reach the core well after the temperature has started to rise.

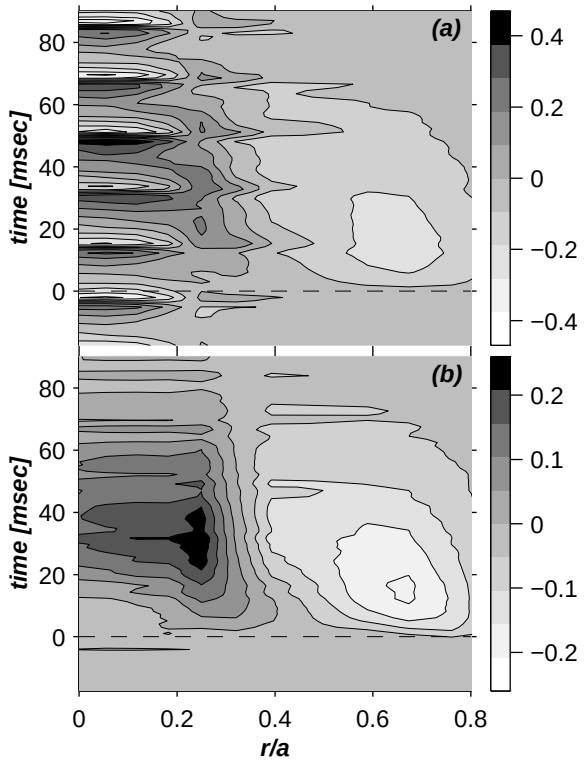

Figure 9: Contour level plot of the temperature amplitude (in absolute units) for shot #21425 with impurity injection. The raw data (a) and the GSVD-corrected data (b) are shown. The injection occurs at $t = 0$ and is marked by a dashed line. Notice the peak in the temperature just outside the inversion radius and the small delay before it enters the plasma core.

The most plausible explanation so far is a modification of the heat diffusivity that is induced by the cold front penetration in the plasma periphery [3, 4, 6, 7, 8]. The exact location at which the cold front triggers the modification is still an open question. In some cases (shot #20792) the central electron temperature doesn't change until the cold front has come close to the inversion radius. Similar observations were made before on other tokamaks, in which different types of stimuli caused the same type of response [35]. In other cases (shot #21425) the initial inward propagation appears to be faster but still the the core temperature takes a few ms to react. This delay is best observed in Fig. 9. We are presently investigating these aspects with predictive transport models [5] and transfer function analyses.

7 Removing sawtooth oscillations with a strong perturbation

To illustrate the limitations of the GSVD, we finally consider shot #21429, in which an obliquely injected pellet causes a rather local but significant density increase in the vicinity of $r/a \approx 0.7$. The resulting perturbation affects both the plasma equilibrium and the sawtooth activity, see Fig. 3. In this example, the noise subset consists of 1050 samples preceding the injection, and the signal subset of the 590 subsequent ones.

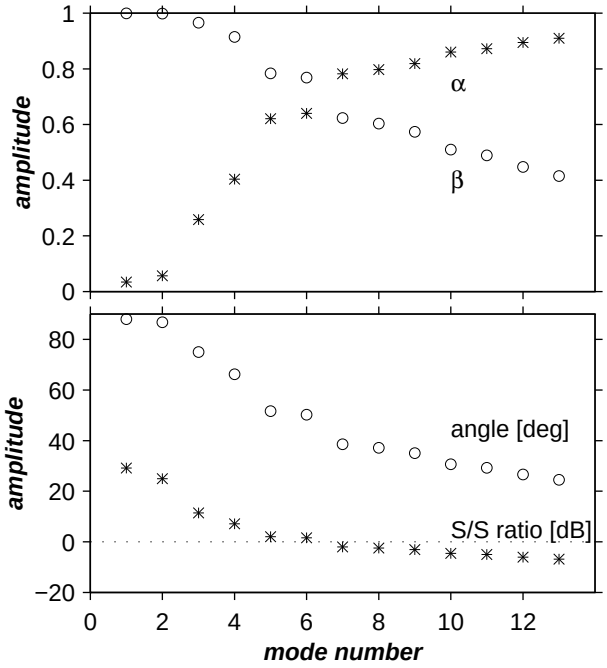

Figure 10: The generalized singular eigenvalues and related quantities for shot #21429. The upper figure shows the weights α_k and β_k and the bottom one the oriented signal-to-signal ratios and separation angles. Several basis vectors point toward both the noise and the signal subspace, attesting an incomplete separation.

Figure 10 shows the existence of some outstanding directions. In contrast to the preceding examples, however, some of the directions do not preferentially favor one of the two subspaces. An inspection of the temporal modes confirms this, see Fig. 11. Modes 1 to 3 mostly capture the pellet-induced perturbation whereas modes 4 to 7 reveal both the initial transient and the large sawteeth that follow. This mixture essentially comes from the nonlinear interaction between the two. Indeed, the sawteeth that immediately follow the injection are affected by the pellet-induced change of confinement. In this case, at least 7 of the 12 modes must be included in order to faithfully reproduce the fast evolution of the temperature profile immediately following the injection. Although the GSVD does bring some improvement over the raw data, it is difficult to reach a compromise between what can be rejected and must be kept.

8 Conclusions

The objective of this paper was to show how the longstanding problem of removing sawtooth oscillations from tokamak data can be successfully solved by means of the Generalized Singular Value Decomposition (GSVD). The technique is sufficiently general to be applicable to other types of experiments in which a predefined coherent or incoherent "noise" has to be removed from multichannel

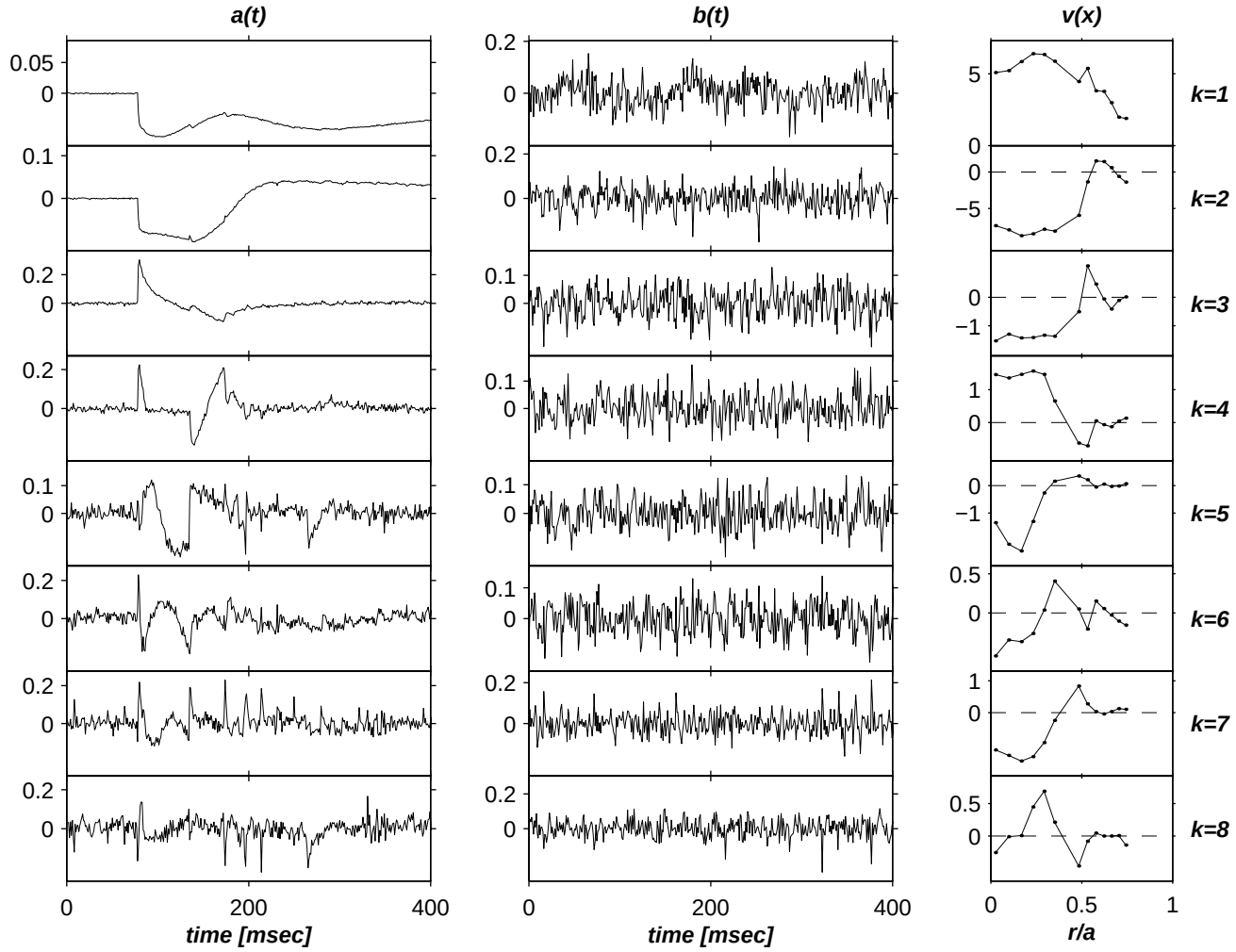

Figure 11: The 8 dominant modes associated with the GSVD for shot #21429. From left to right: the temporal modes $a_k(t)$ of the signal subset, the temporal modes $b_k(t)$ of the noise subset, and the basis vectors $v_k(x)$.

or embedded data. Some examples include the removal of Mirnov oscillations, transients induced by the modulation of additional heating, and instrumental pick-up noise. If the noise is incoherent, then the GSVD reduces to the usual SVD.

Although the linearity of the technique makes its use straightforward, we would like to stress the need for common sense in applying it, since a proper analysis necessarily requires a prior understanding of the noise process one wants to separate from the data. Two necessary conditions are:

1. The noise and the transient response one wants to extract must have different dynamics, otherwise they cannot be separated. This implies that their covariance matrices must have different eigenspaces.

2. The noise must not be significantly affected by the process of interest. The reverse does not have to be true.

These two conditions are usually met in perturbative transport experiments, for which the GSVD is particularly appropriate.

It has been shown how the GSVD considerably eases the analysis of the plasma response to the injection of small amounts of impurities in sawtoothing discharges. The cold front penetration appears with unprecedented clarity and the differing behavior of the central particle and heat transport mechanisms is revealed. The latter is most likely due to modification of the central heat diffusivity shortly (a few ms) after the ablation pulse.

References

[1] H. D. I. Abarbanel, R. Brown, J. J. Sidorowich, and L. Sh. Tsimring, Rev. Mod. Phys. **65**, 1331–1392 (1993).

[2] See *World Survey of Activities in Controlled Fusion Research* (International Atomic Energy Agency, Vienna, 1991) [Nucl. Fusion special supplement (1991)].

[3] K. W. Gentle, W. L. Rowan, R. V. Bravenec, G. Cima, T. P. Crowley, H. Gasquet, G. A. Hallock, J. Heard, A. Ouroua, P. E. Phillips, D. W. Ross, P. M. Schoch, and C. Watts, Phys. Rev. Lett. **74**, 3620–3623 (1995).

[4] M. W. Kissik, J. D. Callen, F. D. Fredrickson, A. C. Janos, and G. Taylor, Nucl. Fusion **36**, 1691–1701 (1996).

[5] M. Erba, A. Cherubini, V. V. Parail, E. Springmann, and A. Taroni, Plasma Phys. Contr. Fusion **39**, 261–276 (1997).

[6] P. Mantica, , M. R. de Baar, J. de Kloe, F. de Luca, P. Galli, G. Gorini, G. M. D. Hogeweij, A. Jacchia, N. L. Lopes Cardozo, A. A. M. Oomens, and the RTP team, "Non-local plasma response induced by peripheral perturbations in the RTP tokamak", in *Proceedings of the 24th European Conference on Controlled Fusion and Plasma Physics, Berchtesgaden, 1997* (EPS, Petit Lancy, in press).

[7] K. W. Gentle, R. V. Bravenec, G. Cima, G. A. Hallock, P. E. Phillips, D. W. Ross, W. L. Rowan, A. J. Wootton, T. P. Crowley, A. Ouroua, P. M. Schoch and C. Watts, Phys. Plasmas **4**, 3599–3613 (1997).

[8] J. D. Callen and M. W. Kissick, Plasma Phys. Contr. Fusion **39**, B173–B188 (1997).

[9] M. Mattioli, C. DeMichelis, and P. Monier-Garbet, Nucl. Fusion **35**, 807–825 (1995).

[10] M. Mattioli, M. Erba, T. Dudok de Wit, A.-L. Pecquet, J.-L. Ségui, and J.-C. Vallet, "Transient regimes of impurity ion transport and electron heat diffusivity in Tore Supra ohmic discharges following nickel laser blow-off injection", Nuclear Fusion, in press.

[11] J.-L. Ségui, P. Gomez, and G. Giruzzi, "An electron cyclotron heterodyne radiometer for measuring the electron temperature", in *Proceedings of the 10th workshop on ECE and ECRH, Ameland, The Netherlands, 1997*, edited by T. Donné (World Scientific, Singapore, to appear).

[12] Ph. Ghendrih, A. Grosman, and H. Capes, Plasma Phys. Contr. Fusion **38**, 1653–1724 (1996).

[13] J.-P. Eckmann and D. Ruelle, Rev. Mod. Phys. **57**, 617–656 (1985).

[14] E. A. Jackson, *Perspectives of nonlinear dynamics* (Cambridge University Press, Cambridge, 1989) vols. I + II.

[15] P. Grassberger, T. Schreiber, and C. Schaffrath, Int. J. Bifurc. Chaos **1**, 521–547 (1991).

[16] H. Kantz and T. Schreiber, *Nonlinear time series analysis* (Cambridge University Press, Cambridge, 1997).

[17] The existence of such trajectories is not necessarily a consequence of the the periodicity of the sawtooth oscillations, since aperiodic, quasiperiodic and chaotic processes may give well-defined trajectories as well. This is actually one of the strong points of the phase space representation.

[18] What we reconstruct here is, strictly speaking, not the true phase space but a space which is topologically equivalent to it. The conditions for obtaining such an equivalence are expressed in the embedding theorems of Whitney and Takens, which play a key role in dynamical systems theory but are less relevant here. See: T. Sauer, J. Yorke, and M. Casdagli, J. Stat. Phys. **65**, 579–616 (1991).

[19] G. H. Golub and C. F. Van Loan, *Matrix computations*, 2nd ed. (The Johns Hopkins Univ. Press, Baltimore, 1988).

[20] D. S. Broomhead and G. P. King, Physica D **20**, 217–236 (1986).

[21] A.-J. van der Veen, E. F. Deprettere, and A. L. Swindlehurst, Proc. IEEE **81**, 1275–1308 (1993).

[22] N. Aubry, P. Holmes, J. L. Lumley, and E. Stone, J. Fluid. Mech. **192**, 115–173 (1988).

[23] D. S. Broomhead, R. Indik, A. C. Newell, and D. A. Rand, Nonlinearity **4**, 159–197 (1991).

[24] C. Nardone, Plasma. Phys. Contr. Fusion **34**, 1447–1465 (1992).

[25] T. Dudok de Wit, R. Lima, A.-L. Pecquet, and J.-C. Vallet, Phys. Plasmas **1**, 3288–3300 (1994).

[26] T. Dudok de Wit, Plasma Phys. Contr. Fusion **37**, 117–135 (1995).

[27] A. Madon and T. Klinger, Physica D **91**, 301–316 (1995).

[28] B. De Moor, Ph. D. dissertation, Katholieke Universiteit Leuven, Leuven, 1988 (unpublished).

[29] E. F. Deprettere, ed., *SVD and signal processing*, (North Holland, Amsterdam, 1988).

[30] G. H. Golub and C. F. Van Loan, SIAM J. Numer. Anal. **17**, 883–893 (1980).

[31] D. Callaerts, B. De Moor, J. Vandewalle, W. Sansen, G. Vantrappen, and J. Janssens, Med. Biol. Eng. Comput. **28**, 217–224 (1990).

[32] C. S. Van Loan, Numer. Math. **46**, 479–491 (1985).

[33] C. C. Paige, SIAM J. Sci. Stat. Comput. **7**, 1126–1146 (1986).

[34] M. Paluš and I. Dvořák, Physica D **55**, 221–234 (1992).

[35] J.-M. Moret, T. Dudok de Wit, B. Joye, and J. B. Lister, Nucl. Fusion **33**, 1185–1200 (1993).